AIChE

Discrete Element Simulation of Free Flowing Grains in a Four-Bladed Mixer

Brenda Remy
Dept. of Chemical and Biochemical Engineering, Rutgers University, Piscataway, NJ 08854

Johannes G. Khinast
Institute for Process Engineering, Graz University of Technology, Graz A-8010, Austria

Benjamin J. Glasser
Dept. of Chemical and Biochemical Engineering, Rutgers University, Piscataway, NJ 08854

DOI 10.1002/aic.11876
Published online June 29, 2009 in Wiley InterScience (www.interscience.wiley.com).

Numerical simulations of granular flow in a cylindrical vessel agitated by a four-blade impeller were performed using the discrete element method. Velocity, density, and stress profiles within the mixer displayed a periodic behavior with a fluctuation frequency equal to that of the blade rotation. Blade orientation was found to affect flow patterns and mixing kinetics. For an obtuse blade pitch orientation, a three-dimensional recirculation zone develops in-front of the blade due to formation of heaps where the blades are present. This flow pattern promotes vertical and radial mixing. No recirculation zone was observed when the blade orientation was changed to an acute blade pitch. The system's frictional characteristics are shown to strongly influence the granular behavior within the mixer. At low friction coefficients, the 3-D recirculation in front of the obtuse blade is not present reducing convective mixing. Higher friction coefficients lead to an increase in granular temperature which is associated with an increase in diffusive mixing. Normal and shear stresses were found to vary with mixer height with maximum values near the bottom plate. Additionally, a strong dependence between the magnitude of the shear stresses and the friction coefficient of the particles was found. The stress tensor characteristics indicate that the granular flow in our simulations occurs in the quasi-static regime. At the same time, the averaged pressure was found to vary linearly with bed height and could be predicted by a simple hydrostatic approximation. © 2009 American Institute of Chemical Engineers *AIChE J,* 55: 2035–2048, 2009

Keywords: bladed mixer, DEM, granular mixing, agitated dryer, quasi-static flows

Introduction

Particulate processing operations in a wide variety of industries are often poorly understood compared with their fluid processing counterparts. This reality stems in part from the fact that we lack a set of constitutive equations derived from first-principles that describe granular flows under a specified initial state and boundary conditions. The lack of fundamental understanding of granular systems leads to broad assumptions during process design, poor identification of critical process parameters, and scale-up complications which are not easily explained.[1] Traditionally, heuristic rules-of-thumb have been used to limit these problems, but these have not reliably prevented complications, such as

Correspondence concerning this article should be addressed to B. J. Glasser at bglasser@rutgers.edu

nonuniform flow and segregation, from occurring during scale-up or commissioning.

Despite the complexity surrounding granular flows, a large number of industrial processes involve the transport, mixing, and storage of particulate systems. Industrially relevant geometries tend to be more complex than the simple shear flows which have been extensively studied in the literature. The cylindrical mixer geometry mechanically agitated by an impeller is common in a variety of particle processing technologies. Although in many cases, agitated mixers are used to homogenize a blend of solid particles, they also serve to enhance heat and mass transfer (e.g., agitated dryers). Similar equipment is also used in high-shear granulation processes and in tablet press operations to encourage flow in the feed-frame assemblies. Although simple in form, the mechanisms by which particle motion is generated in cylindrical mixers are still poorly understood. Problems, such as segregation, particle attrition, and agglomeration[2–4] are known to occur in this geometry but the role of operating parameters and particle properties on flow behavior remains unclear.

Early experimental studies in this geometry focused on the power and torque requirement on two-dimensional flows to determine strain rates at the failure point.[5,6] These studies found the existence of particle recirculation patterns that move with the blade. Horizontal cylindrical mixer studies were performed by Malhotra et al.,[7–9] Laurent et al.,[10] Jones et al.[11] and Bridgwater et al.[12] The studies by Malhotra focused on two-dimensional geometries and provide information on mixing kinetics and heat transfer coefficients for agitated dryers. Laurent et al.[10] found that flows in this geometry are periodic in nature, whereas Jones et al.[11] observed slower mixing when the fill level was increased. Bridgwater et al.[12] observed the development of three-dimensional recirculation zones in a ploughshare (horizontal) mixed above a critical impeller speed. A three-dimensional picture of flows over two flat blades emerged with the use of positron emission particle tracking. Three-dimensional recirculation zones were observed and the size of some of these zones varied significantly with fill level.[13] Additionally, the velocity profiles inside the mixer were found to vary linearly with the rotational speed of the blade. A more complex blade configuration was studied utilizing particle image velocimetry.[14,15] This technique records particle positions at the free surface and near transparent walls which allows for the characterization of the flow fields and the determination of particle trajectories. The particle movement within the mixer was found to be periodic and its frequency depended on the speed of the blade rotation, a behavior similar to what was found in horizontal mixers. Striation patterns that developed through stretching and folding were observed for low-shear operations which were consistent with chaotic granular mixing. This behavior was not present during high-shear operations.

Experimental studies have provided insight into the granular behavior in bladed mixers, but these studies have been limited to the effect of a small set of process parameters and particle properties on the measured variables. The set of measured parameters was in turn limited by the capabilities of the analytical techniques used. Numerical simulation techniques have the potential of bridging the knowledge gap, as they allow for the study of parameters that are difficult to measure or vary experimentally. The discrete element method (DEM) has been widely used in recent years to examine granular flow in a variety of systems ranging from simple shear flows to more complex, industrially relevant geometries. These studies have provided insight into the system's dynamics and transient behavior. With this technique, information can be obtained on local flow and stresses that are difficult, if not currently impossible to obtain experimentally. Stewart et al.[16] and Zhou et al.[17,18] performed numerical studies using DEM for bladed mixers with two flat blades. These studies focus on the effect of particle friction, size distribution, and particle density on the flow and segregation patterns that developed inside bladed mixers. The particle's frictional characteristics were found to affect velocity profiles and mixing kinetics, whereas particle size and particle density affected segregation patterns. Sinnott and Cleary[19] performed three-dimensional DEM simulations and investigated the effect of different blade configurations on granular mixing. Two configurations were studied: a flat rectangular blade and a horizontal bottom disc. The authors found that the degree of mixing was susceptible to blade configuration.

These studies have complemented our understanding of three-dimensional flow structures but have not clearly correlated operating parameters and particle properties to macroscopic properties like density, pressure, stress, and granular temperature. Knowledge of how particle properties affect macroscopic properties is important for the effective operation, scale-up and design of bladed mixers. Although previous work has shown that particle friction is an important parameter, the effect of friction on the mentioned macroscopic properties is still not fully understood. Additionally, little is currently known about the stress evolution in bladed mixers and the parameters that affect it. High-shear granulation processes depend on stresses developed via agitation to achieve controlled agglomeration and attrition of granules. In contrast, agitated drying processes in the pharmaceutical industry are generally designed to minimize the effect of attrition and agglomerate formation due to shearing. Uncontrolled shearing could lead to broad particle size distributions, formation of fines or large agglomerates, and even loss of crystallinity.

The numerical studies performed for bladed mixer thus far have focused on relatively simple blade configurations. More industrially relevant blade configurations remain to be examined and it is uncertain, whether the results obtained with the simplified geometries can be extended to the more complex industrial cases. The work presented here focuses on the computational examination of granular flow for cohesionless, monodisperse spheres in a cylindrical mixer agitated by four blades pitched at a 45° angle. This geometry is representative of several industrial granular processes, including filter dryers and high-shear granulators. The goal of this study is to provide a three-dimensional picture of granular behavior including flow patterns, mixing kinetics, bulk density, granular temperature, pressure, and shear-stress profiles. We examine the effect of blade orientation, sliding friction, and shear rates on the temporal and spatial averages of these parameters as well as fluctuating values. We compared our results to previously reported experimental and computational results. The findings presented are relevant to the operation and optimization of industrial processes as they provide insight on parameters that may affect mixing, segregation, heat transfer, particle attrition, and particle agglomeration.

Numerical Method

Discrete element method

DEM considers interparticle contacts to describe the behavior of a particulate system. It integrates Newton's equations of motion for each particle starting from an initial system configuration. If the time-step for integration is sufficiently small, it can be assumed that the state of a particle is only affected by the contact with its neighbors. Thus, at any given time-step, the discrete element method considers only pair-wise interactions of neighboring particles. This method provides information regarding the particle's position, velocity, and resultant forces. The motion of each particle is described by

$$m_i \frac{dv_i}{dt} = \sum_j (F_{ij}^N + F_{ij}^T) + m_i g \tag{1}$$

$$I_i \frac{d\omega_i}{dt} = \sum_j (R_i \times F_{ij}^T) + \tau_{rij} \tag{2}$$

where m_i, R_i, I_i, v_i, and ω_i are the mass, radius, moment of inertia, linear velocity, and angular velocity of particle i, and g is the acceleration due to gravity. The contact model used in this work is based on the work of Tsuji et al.,[20] which provides a nonlinear force based on Hertzian contact theory. The normal contact force is given by

$$F^N = -\widetilde{k}_n \delta_n^{3/2} - \tilde{\gamma}_n \dot{\delta}_n \delta_n^{1/4} \tag{3}$$

where $\widetilde{k}_n$ is the normal stiffness coefficient, δ_n is the normal displacement, and $\widetilde{\gamma}_n$ is the normal damping coefficient. The normal stiffness coefficient is obtained from

$$\widetilde{k}_n = \frac{E\sqrt{2R^*}}{3(1-\sigma^2)} \tag{4}$$

with E being the particle's Young's modulus and σ the particle's Poisson ratio. R^* is defined as the effective radius of the contacting particles and is obtained by

$$R^* = \frac{R_i R_j}{R_i + R_j}. \tag{5}$$

The normal damping coefficient is given by

$$\widetilde{\gamma}_n = \ln e \frac{\sqrt{m\widetilde{k}_n}}{\sqrt{\ln^2 e + \pi^2}} \tag{6}$$

where e is the coefficient of restitution. This model assumes a constant coefficient of restitution and results in a velocity-dependent collision time. Although experimental data suggest an impact-velocity dependent coefficient of restitution, this model has been shown to produce DEM results in good agreement with experimental data[20–23] and comparable with other commonly used contact models.[24,25]

The tangential force is calculated from

$$F^T = -\widetilde{k}_t \delta_t - \widetilde{\gamma}_t \dot{\delta}_t \delta_n^{1/4} \tag{7}$$

where $\widetilde{k}_t$ is the tangential stiffness coefficient, δ_t is the tangential displacement, and $\widetilde{\gamma}_t$ is the tangential damping coefficient. The tangential stiffness coefficient is based on the work from Mindlin[26] and is given by

$$\widetilde{k}_t = \frac{2\sqrt{2R^*}G}{2-\sigma} \delta_n^{1/2} \tag{8}$$

where G is the particle's Shear modulus. The tangential displacement is calculated by

$$\delta_t = \int v_{rel}^t dt \tag{9}$$

where v_{rel}^t is the relative tangential velocity of the colliding particles and is defined as

$$v_{rel}^t = (v_i - v_j) \cdot s + \omega_i R_i + \omega_j R_j \tag{10}$$

In Eq. 10, s is the tangential decomposition of the unit vector connecting the center of the particle. The tangential force is limited by the Coulomb condition, $F^T < \mu_s |F^N|$. When the tangential force obtained from Eq. 7 exceeds the Coulomb limit, the tangential displacement is set to $\delta_t = F^T/\widetilde{k}_t$ to account for slip during a contact. It is interesting to note that as a consequence of setting δ_t equal to $F^T/\widetilde{k}_t$, δ_t is always less than $F^N/\widetilde{k}_t$. The effect of rolling friction is included in the term $\tau_r = -\mu_r |F^N| R\omega$. In this work, the tangential damping coefficient is assumed to be the same as the normal damping coefficient.

Input parameters and mixer geometry

The input parameters for our simulations are listed in Table 1 and are, in general, those of glass. The sliding friction coefficient was varied from that of glass to examine the effect of this parameter on the granular behavior. Additionally, the value of Young's modulus was decreased to reduce computational time. Parametric sensitivity studies showed that reducing the value of Young's modulus had a negligible effect on flow patterns, velocity profiles, and interparticle shear stresses. These observations are consistent with the literature.[16–18,27] The parametric studies also showed that the amount of viscous dissipation in the normal and tangential directions had a negligible effect on the results obtained in our bladed mixer. The maximum normal overlap observed in the simulations was 4% and the averaged overlap was <1%. The physical properties listed in Table 1 were used for the particles, the blades, and cylinder walls.

The mixer dimensions used in this work are shown in Figure 1. In our coordinate system, the origin is located at

Table 1. Input Parameters

Variable	Symbol	Value
Rolling friction coefficient	μ_r	0.005
Sliding friction coefficient	μ_s	0.1–0.5
Particle density	ρ	2.2 g/ml
Young's modulus	E	2.6×10^6 Pa
Coefficient of restitution	e	0.6
Particle diameter (d)	d	5–10 mm
Number of particles	N	5,000–36,000
Poisson's ratio	σ	0.25
Time step		$<1 \times 10^{-5}$ s

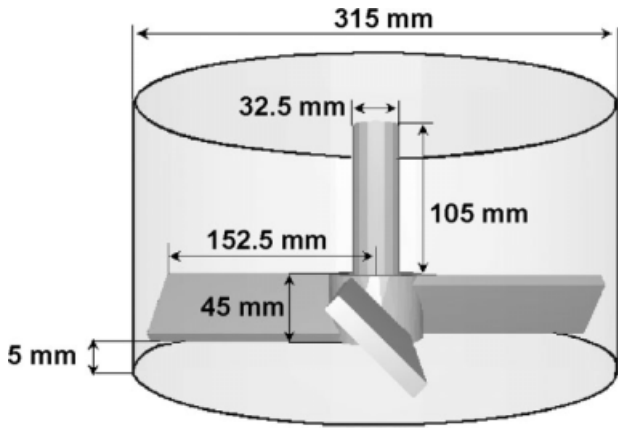

Figure 1. Mixer dimensions.

the center of the cylinder's bottom plate. The amount of particles in each simulation was set such that the top of the particle bed covered the height of the blades. The particle bed was composed of monodisperse, cohesionless spheres. Two different particle sizes were used 5 and 10 mm. The 5 mm particles were used to characterize flow structures and velocity fields for different blade orientations, whereas the 10 mm particles were used to examine the effect of friction and shear rate. The larger, 10 mm particles were used to reduce computational time. The change in particle size did not have an effect on the flow patterns observed in the simulations. Comparisons of results between simulations are done while keeping the ratio of particle diameter to mixer diameter constant.

Simulations were performed using blade speeds ranging from 10 to 30 revolutions per minute (RPM). Particles are created in the computational space and allowed to settle under gravity while the blades remain stationary. Blade movement is started once particle deposition has been completed. Measurements are taken after the system has reached steady state. The system is considered to be at steady state when the total kinetic energy of the system reaches a constant value, indicating that the amount of energy lost due to inelastic collisions is the same as the amount of energy gained from the movement of the blade. Under these conditions, steady state is reached within 2 s of blade movement.

Results and Discussion

Effect of blade orientation

We begin by characterizing the flow of granular material for different blade orientations. For the blade configuration shown in Figure 1, the granular material can be sheared at two different blade pitches. By rotating the blades counter-clockwise, the blade pitch relative to the movement of particles has an obtuse angle. This blade orientation is most common in particulate processing equipment. Rotating the blade clockwise produces an acute blade pitch. Although less common, this blade orientation is used in industrial processing during unloading operations or smoothing of beds in filter dryers. A counter-clockwise rotation is denoted by a positive tangential velocity; a clockwise rotation is denoted by a negative tangential velocity. We compare the flow structures and highlight the differences obtained for each configuration. The blade speed for both blade orientations was set to 20 RPM. The results listed in the following sections were obtained using 5 mm particles with sliding friction coefficients (μ_s) of 0.3.

Velocity profiles

Instantaneous velocity profiles at radial position $r = 0.09$ m and height $h = 0.06$ m are shown in Figure 2 for the obtuse and acute blade pitches. A cubic control volume with a size of six particle diameters was created at these coordinates. This position was chosen as the control volume would be located halfway between the impeller shaft and the cylinder wall and would include particles above and within the span of the blades. The velocity components were calculated by averaging over the control volume at a particular time-step. The velocity profiles in Figure 2 show a periodic behavior for both the obtuse and acute blade pitches. A Fast Fourier Transform (FFT) analysis of the tangential velocity component (V_t) revealed that the main frequency of this fluctuation is 1.3 Hz which corresponds to the rotation frequency of the blades. This analysis was carried out using the Fast Fourier Transform algorithm in *MATLAB*. The same main frequency was obtained when this analysis was extended to the radial (V_r) and vertical velocities (V_y). This periodic behavior was observed experimentally by Lekhal et al.[2] for velocity surface measurements. Here we are able to track velocity fluctuations throughout the particle bed. The power spectrum obtained from this analysis is shown in Figure 2d for the obtuse blade pitch and Figure 2h for the acute blade

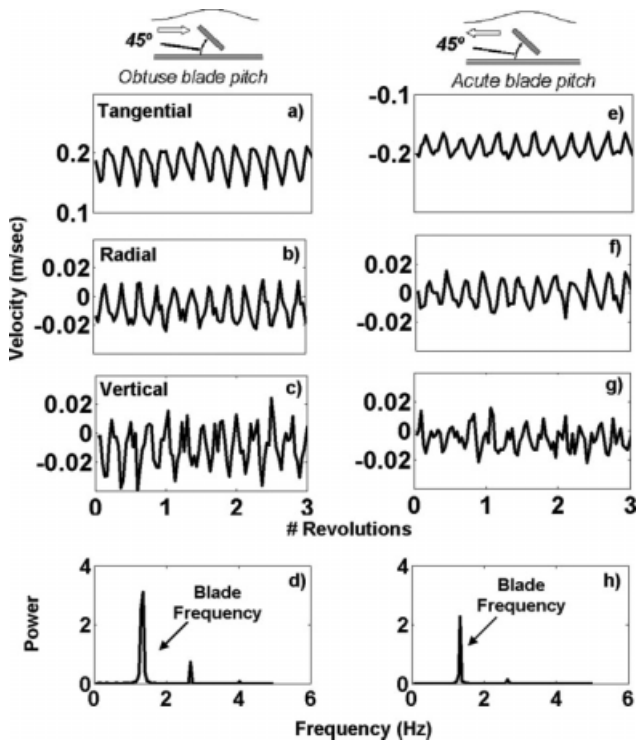

Figure 2. Velocity profiles at $r = 0.09$ m, $h = 0.06$ m.

Obtuse blade pitch: (a) tangential, (b) radial, (c) vertical velocity, and (d) tangential velocity power spectrum. Acute blade pitch: (e) tangential, (f) radial, (g) vertical velocity, and (h) tangential velocity power spectrum.

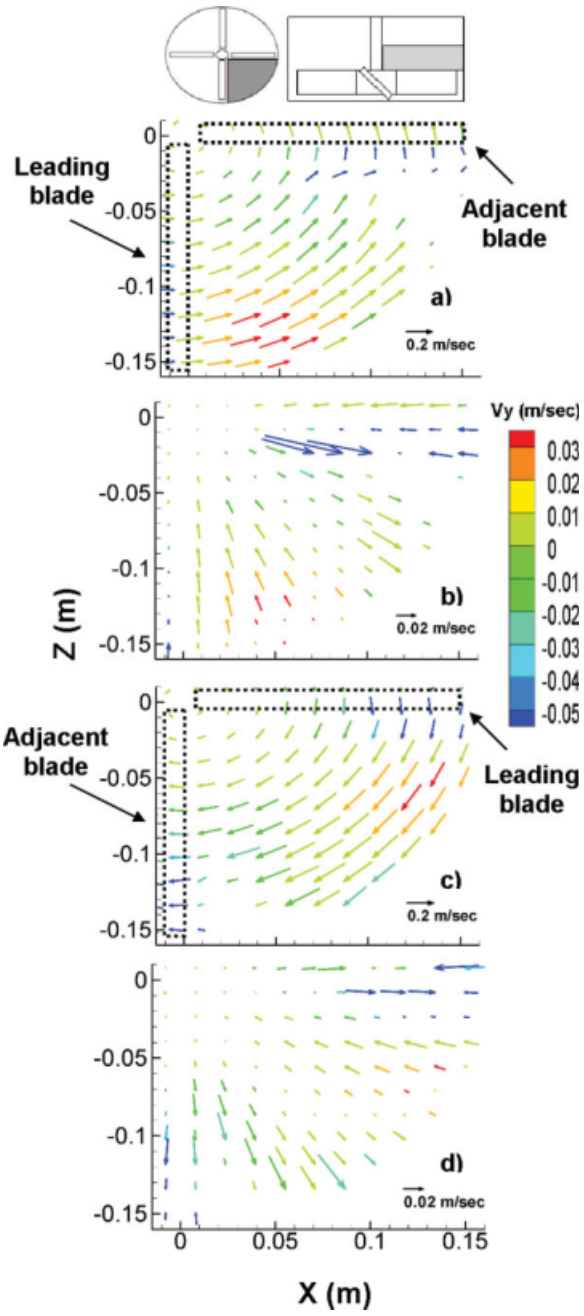

Figure 3. Time-averaged velocity fields on horizontal plane

Obtuse blade pitch: (a) tangential velocity and (b) radial velocity. Acute blade pitch: (c) tangential velocity and (d) radial velocity. [Color figure can be viewed in the online issue, which is available at www.interscience.wiley.com.]

pitch. The intensity of the main peak for the obtuse blade pitch is higher than that of the acute blade pitch indicating a higher fluctuation amplitude. The particle movement in the tangential direction is therefore less uniform for the obtuse blade pitch than for the acute blade pitch.

The tangential velocity for both blade configurations is one order of magnitude higher than the radial and vertical velocities. Particle movement in this system is therefore dominated by the angular movement of the blade. Radial and vertical velocity values fluctuate around zero, whereas the tangential velocity does not. This indicates that the position of the particles relative to the blade determines if particles rise or fall or if they flow toward the cylinder wall or toward the impeller shaft. The amplitude of the radial and vertical fluctuations is higher for the obtuse blade pitch than for the acute blade pitch. As in the tangential direction, particle flow in the radial and vertical directions is less uniform for the obtuse blade pitch configuration.

Although the main flow of the particles in this system is in the tangential or angular direction, complex flow structures are observed. As the blades rotate, the granular bed deforms by forming heaps where the blades are present and valleys between blades passes. Figure 3 depicts time-averaged velocity fields for particles above the blades in the horizontal plane. Averaging was performed considering only the time-steps for which the blades were present at the position shown in Figure 3. Figures 3a, c show the horizontal plane velocity field for the obtuse and acute blade pitch, respectively. The color of the vector represents the value of the vertical velocity. The velocity fields for the obtuse and acute cases are very similar with the main difference being the direction of flow. As expected, the magnitude of the velocity increases for particles close to the wall. Additionally, the velocity is higher for particles near the front of the leading blade than for particles behind the adjacent blade. For the vertical velocity, the magnitude is highest by the wall while particles near the shaft have a small vertical velocity component. This trend is observed for both blade orientations. The radial velocity fields are presented in Figure 3b for the obtuse blade pitch and 3d for the acute blade pitch. Particle radial movement is limited for the acute blade pitch, whereas higher radial velocities are observed for the obtuse blade pitch. Similar to the vertical velocity, the magnitude of the radial velocity is highest by the cylinder wall and smallest near the shaft.

The radial and vertical velocity trends shown in Figures 2 and 3 suggest the existence of three-dimensional recirculation patterns. These patterns are observed in the velocity fields obtained in the vertical plane (Figure 4). Figures 4a–c show the time-averaged radial and vertical velocity fields for the obtuse blade pitch at three different positions. The magnitude of the tangential velocity is represented by the color of the vectors. For the obtuse blade pitch, the tangential velocity points out of the plane of the graph. In front of the blade (Figure 4a), a recirculation pattern develops analogous to the vortexing observed for liquid systems in cylindrical tanks agitated by pitch-blade turbines.[28] Experimental surface flow measurements suggested the existence of a 3D recirculation zone.[14] Our computational results confirm the existence of this zone and describe where and how the recirculation develops. A less prominent recirculation pattern was reported by Zhou et al.[18] for two flat blades. In particular, the velocity for the particles near the bottom plate and the shaft was significantly smaller than what is observed in our system. In our system, the recirculation is much stronger as due to the pitch of the blade, the particles by the wall flow upward forming a heap. The particles on the top of the heap move radially inward which forces the particles by the shaft to flow downward and radially outward, leading to the pronounced recirculation. The existence of such recirculation

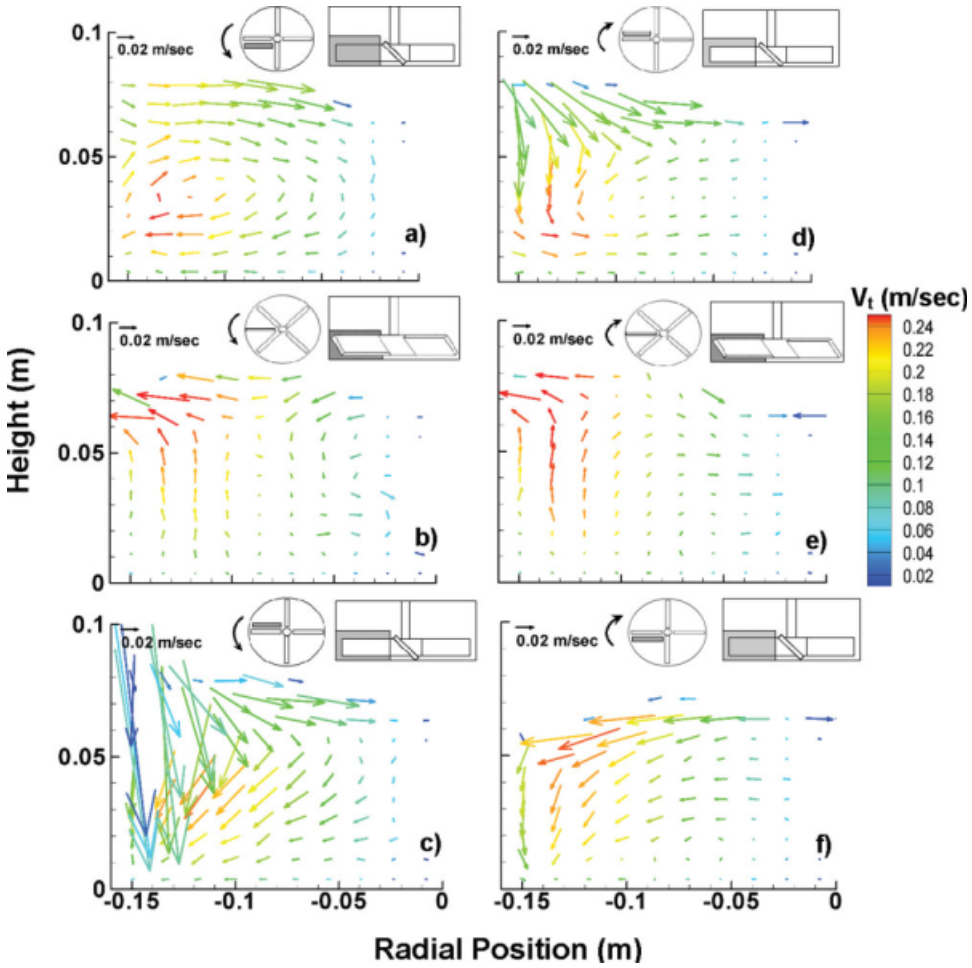

Figure 4. Time-averaged radial and vertical velocity fields in the vertical plane.

Obtuse blade pitch: (a) front of blade, (b) in-between blades, and (c) behind the blade. Acute blade pitch: (d) front of blade, (e) in-between blades, and (f) behind the blade. [Color figure can be viewed in the online issue, which is available at www.interscience.wiley.com.]

patterns becomes important during process design and scale-up, as such patterns could lead to enhanced mixing in monodisperse systems and potentially in polydisperse systems as well. Unlike liquid systems, this recirculation pattern is only present near the front of the blade. In between the blades, the particles on top of the blades now flow radially outward (Figure 4b) whereas particles by the bottom plate and shaft move mainly in the tangential direction. Particles by the wall flow upward with a small radial velocity component. As the blade passes, particles on the top of the heap fall behind the blade (Figure 4c). Particles within the blade height flow downward as they fall from the front of the heap similar to forward flowing avalanches.

The acute blade pitch velocity profiles are shown in Figures 4d, f. In this case, the tangential velocity points into the plane of the graph and the magnitude is represented by the vector color. No recirculation pattern arises in front of the blade (Figure 4d) contrary to what is observed for the obtuse blade pitch. Particles by the cylinder wall flow downward due to the blade's pitch. Particle on top of the blade flow radially inward. A "dead zone" can be noticed near the shaft and bottom plate, as these particles have a small tangential velocity component and almost no vertical or radial movement. This "dead zone" is present in between the blades (Figure 4e) and behind the blade (Figure 4f). The presence of this "dead zone" has a significant effect on the mixing performance for the acute blade pitch, as will be demonstrated in the Mixing kinetics Section. Particles by the wall follow the same behavior in between the blades and behind the blade as in the obtuse blade pitch case (Figures 4e, f).

Density and granular temperature profiles

The bulk density of a system and the granular temperature profile are important macroscopic properties of a granular assembly. Knowledge of how these profiles develop in dynamic systems could assist in the development of continuum-like models analogous to classical thermodynamic theory. Bulk density measurements provide insight into the system's compression and dilation states and can help determine other macroscopic properties such as pressure. The granular temperature is defined as $T = 1/2\langle u'u'\rangle$, were u' is the fluctuation velocity, which is the instantaneous deviation from the mean velocity in a control volume around the point being examined. $\langle\ \rangle$ denotes the temporal averaging of the quantity $u'u'$ within the control volume. Granular temperature profiles

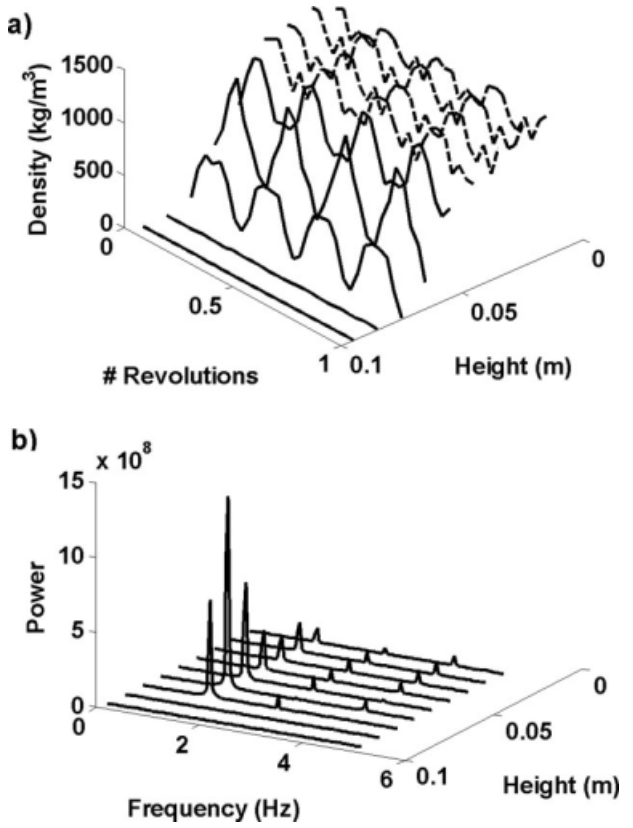

Figure 5. Density fluctuations at $r = 0.09$ m for the obtuse blade pitch.

(a) Density profile as a function of revolution and height, (b) density fluctuation power spectrum as a function of height.

could be used to gauge the diffusive behavior of particles[29] and the tendency of the system to segregate as temperature gradients have been shown to produce segregation.[30]

Periodic bulk density waves are seen within the mixer (Figure 5). As in the velocity case, the main density fluctuation frequency is that of the blades' rotation. This behavior indicates that the granular material compresses as the blade passes and dilates in between the blades. It is worth noting that qualitative differences in particle packing as a function of blade position were observed experimentally by Stewart et al.[13] The DEM simulations allow us to quantify the frequency and magnitude of the density waves. Density profiles for the obtuse blade pitch as a function of mixer height and number of revolutions are shown in Figure 5a at $r = 0.09$ m. The average density and the amplitude of the fluctuations are a function of the mixer height. The power spectrums corresponding to these density profiles are shown in Figure 5b. The main peak height in the power spectrums shows that the amplitude of the fluctuations remains constant within the region that spans the height of the blades. In this region, the bulk density fluctuates between a maximum value of 1300 kg/m^3 and a minimum value of 1000 kg/m^3. This maximum value is close to the randomly close-packed density ($\sim$1400 kg/m^3 in this case). Above the blades, the mean value and amplitude of these fluctuations change significantly. At $h = 0.055$ m, the density fluctuates between 1300 and 800 kg/m^3. The highest fluctuation amplitude occurs at $h = 0.065$ m, where density values range from 1200 to 300 kg/m^3. This region coincides with the top of the heaps. The granular material begins to compress at the leading edge of the heap and dilates as the particles fall in the wake of the blades. The magnitude of the density minima in this region suggests that the particle concentration in the wake of the blade is small. We may think of particles in this region as being fluidized for the period required for the wake of the blade to pass. The smallest density values are observed at the heap's summit ($h = 0.075$ m) as particle concentration here is at its lowest. The amplitude of these fluctuations is similar to that at $h = 0.055$ m.

A similar trend in density fluctuations is observed in the acute blade pitch case. However, differences in the average bulk densities were found. For the obtuse blade pitch, the total average bulk density was measured at $\sim$900 kg/m^3 whereas for the acute blade pitch the total average bulk density was found to be $\sim$1100 kg/m^3. The difference in bulk density can be explained by the blade configuration in each case. In the obtuse blade pitch configuration, the blade movement acts against gravity lifting the granular material up and causing dilation. On the other hand, the acute blade pitch acts in the same direction as gravity compressing the granular material as it gets pushed down. It should be noted that bed dilation relative to initial conditions ($\sim$1200 kg/m^3 initial density) also occurs for the acute blade pitch but to a lower extent than for the obtuse blade pitch. The difference in bulk density affects the stress profile within the granular bed, as will be shown in the Shear and normal stress profiles section.

The time-averaged granular temperature profiles are shown in Figure 6. Figures 6a, c show contour plots of the granular temperature in the horizontal plane for the obtuse and acute blade pitch, respectively. Vertical plane profiles are shown in Figures 6b, d. Granular temperature maximums are observed near the cylinder wall (Figure 6a) and above the top tip of the blades (Figure 6b). These high temperature regions correspond to the areas where the particle velocity is the highest (as shown in Figures 3 and 4). Additionally, frictional interactions between the particles and the cylinder wall leads to an increase in granular temperature. The resulting velocity of wall-colliding particles differs from that of the bulk flow due to wall friction. This behavior is also observed in granular flows down inclined chutes, where the granular temperature is highest by the rough chute wall.[31] Lower temperature regions exist near the impeller shaft and within the span of the blades. These colder regions represent areas of uniform particle flow and low velocity fluctuations. Similar granular temperature trends in the horizontal plane were observed experimentally by Lekhal et al.[15] via surface velocity measurements. The granular temperature for the acute blade pitch is much lower than for the obtuse blade pitch (Figures 6c, d). This is consistent with the velocity fluctuation results presented in the Velocity profiles section. The acute blade orientation leads to more uniform flows where the bulk of the particles follow the angular motion of the blade. For this case, granular temperature mostly is generated by the frictional interactions with the cylinder wall and the bottom plate.

Mixing kinetics—Obtuse vs. acute pitch

The differences in granular behavior observed between the obtuse and acute blade configurations lead to differences in

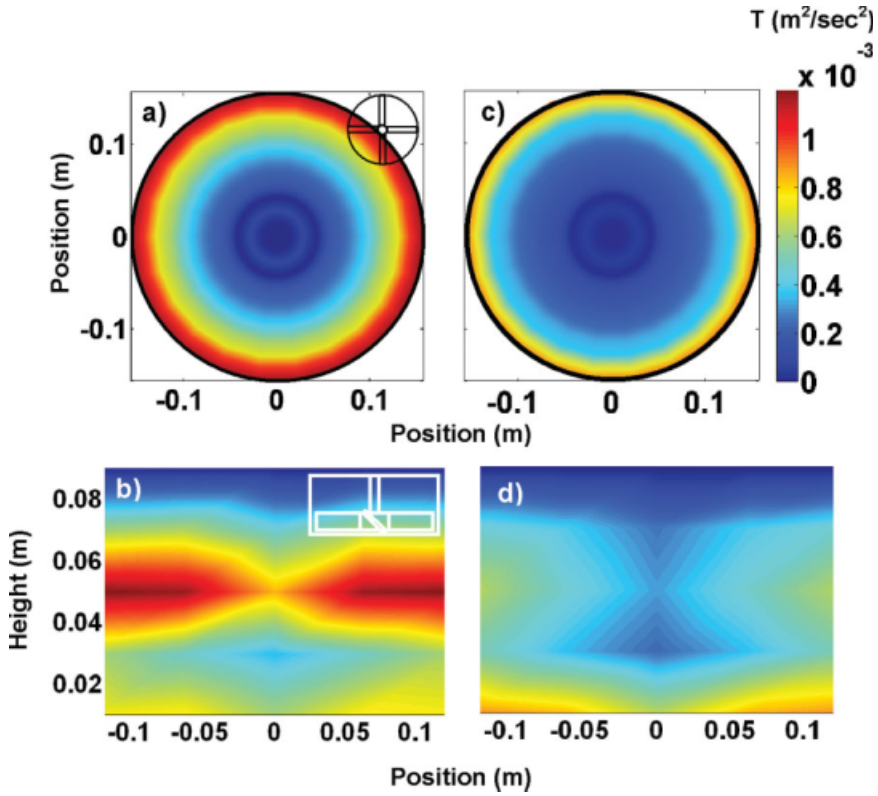

Figure 6. Time-averaged granular temperature profiles.

Obtuse blade pitch: (a) horizontal plane and (b) vertical plane. Acute blade pitch: (c) horizontal plane and (d) vertical plane. [Color figure can be viewed in the online issue, which is available at www.interscience.wiley.com.]

mixing performance. We evaluate the degree of mixing obtained for each blade orientation by coloring particles on the left side of the horizontal plane differently from the particles on the right side prior to blade movement. The particles have identical properties except their color. We then follow the mixing pattern as blade motion begins. In addition, we perform statistical analysis on particle concentration for a specific color particle. At a particular time step, we compute the relative standard deviation (RSD) of particle concentration for the entire system. The RSD is obtained from the following formula:

$$\mathrm{RSD} = \frac{\sigma_{\mathrm{conc}}}{M_{\mathrm{conc}}} \tag{11}$$

where σ_{conc} is the standard deviation of the particle concentration over all the samples taken and M_{conc} is the overall mean particle concentration. The RSD value obtained can be highly sensitive to sample size and sample number. The sample grid size for the RSD calculation was determined by varying the sample number and size until the RSD value obtained was independent of sampling grid.

Figure 7 shows snapshots of the top horizontal plane view for the obtuse blade pitch (Figure 7a) and for the acute blade pitch (Figure 7b) at different numbers of revolutions. Well-mixed zones in both cases are first observed by the cylinder wall, the area of highest granular temperature. Thus, the frictional characteristics of the wall facilitate mixing by increasing the fluctuation velocities. In contrast, areas of uniform flow and lower granular temperature remain unmixed for longer periods of time. Enhanced mixing is obtained for the obtuse blade pitch when compared with the acute blade pitch. This mixing difference is observed as early as after 1 revolution. After 4 revolutions, the obtuse blade pitch system is well mixed and mixing is down to the particle–particle level, whereas unmixed regions still remain in the acute blade pitch system. The velocity profiles showed that for acute blade pitch flows, "dead zones" appear and the 3-D recirculation found for the obtuse blade pitch is not present. Convective mixing is reduced by agitating with an acute blade pitch. Additionally, the acute blade pitch leads to a lower granular temperature within the particle bed. This decrease in granular temperature is associated with a decrease in particle diffusivity. Diffusive mixing is therefore hindered by acute blade pitch flows. The difference in mixing performance is confirmed with the calculation of the system's RSD (Figure 8). After 5 revolutions, the RSD for the obtuse blade pitch is 0.45 whereas for the acute blade pitch is 0.51, indicating that higher number of unmixed regions exist in the acute blade pitch case. The difference in mixing performance is still present after 10 revolutions.

Effect of microscopic friction

Previous work done on bladed mixers with two flat blades showed that particle friction is an important parameter.[16,18] In this section, we look at the effect of sliding friction on velocity fields, density and granular temperature profiles, and

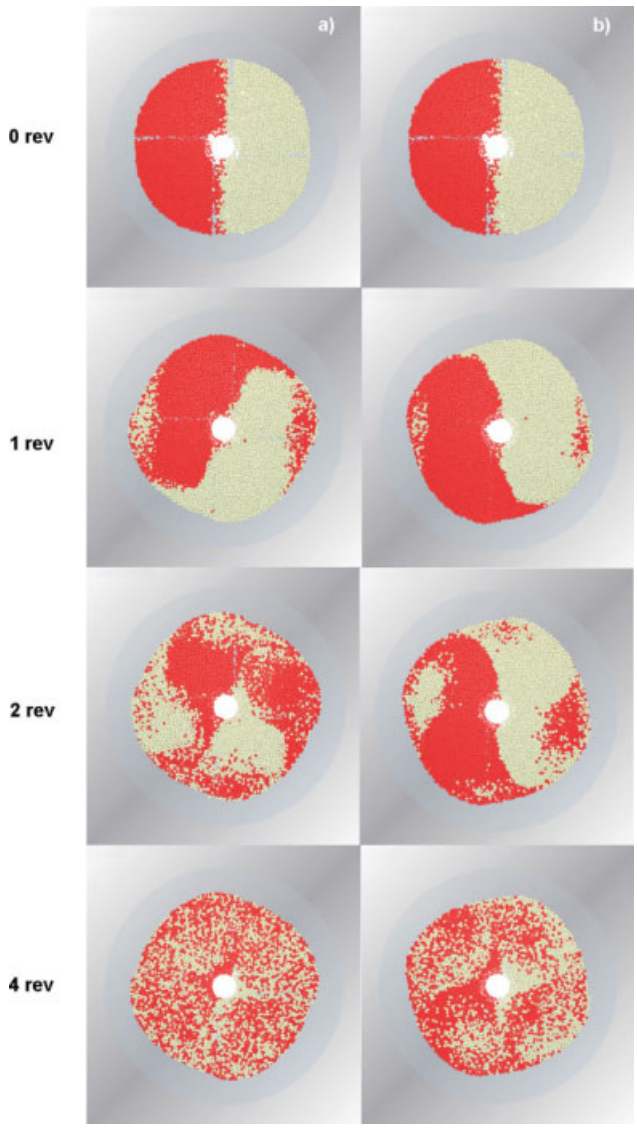

Figure 7. Top view of mixing for left-right segregated system at 20 RPM.

(a) Obtuse blade pitch and (b) acute blade pitch. [Color figure can be viewed in the online issue, which is available at www.interscience.wiley.com.]

mixing kinetics. To reduce computational time, the results listed in this section were obtained using 10 mm particles. We find that similar flow patterns and trends are obtained for the 10 mm particle vs. the 5 mm particles. The simulations outlined in this section were carried out for an obtuse blade pitch and a rotational speed of 10 RPM.

From the system's frictional properties, the sliding friction coefficient (μ_s) was found to significantly affect velocity trends while the rolling friction coefficient (μ_r) had a negligible effect. Velocity fields at the front of the blade in the vertical plane are presented in Figure 9 for three different values of μ_s. Heap formation occurs for $\mu_s = 0.5$ and $\mu_s = 0.3$ (Figures 9a, b, respectively) leading to the formation of the three-dimensional recirculation zone. At these frictional conditions, stable contact force chains develop between particles,[32] which cause the particle bed to deform by forming heaps where the blades are present. A force chain is a network of interparticle contacts in which force is transmitted along the contact path. Little difference is observed between the velocity fields shown in Figures 9a, b. Particles rise by the wall and fall by the impeller shaft. When μ_s is set to 0.1 (Figure 9c) a different behavior is observed. Because of the low friction, stable contact force chains do not form, particles slide past each other more often and no heap is formed. This in turn leads to low radial and vertical velocity values and the recirculation zone cannot develop. Particles move as a block solely in the tangential direction. A similar behavior was observed at low sliding friction coefficients for a flat two-blade impeller configuration.[18] However, experimental verification of the low friction results is still needed.

Bulk density differences were also observed. The vertical and radial movement of the particles for $\mu_s = 0.5$ and $\mu_s = 0.3$ allow the granular bed to dilate as the blade moves, leading to a total average bulk density value of $\sim$900 kg/m^3. In contrast, little bed dilation is observed for the case of $\mu_s = 0.1$. The average bulk density in this case was measured at $\sim$1200 kg/m^3. Density fluctuations similar to the ones shown in Figure 5 were observed for all values of μ_s. However, the mean and amplitude for the $\mu_s = 0.1$ case are not dependent on mixer height. The density in this case fluctuates between 1300 kg/m^3 and 1000 kg/m^3.

Fluctuation velocities are also affected by the value of μ_s. Figure 10 shows the time-averaged granular temperature profiles as a function of radial position for the three values of μ_s. Increasing the value of μ_s leads to an increase in the granular temperature of the system. Granular temperature gradients are observed for $\mu_s = 0.5$ and $\mu_s = 0.3$. However, a colder and uniform granular temperature profile is obtained for the $\mu_s = 0.1$ case. As a result, periodic velocity fluctuations are seen for $\mu_s = 0.5$ and $\mu_s = 0.3$ but not for $\mu_s = 0.1$ (not shown). Increasing the sliding friction coefficient leads to an increase in velocity fluctuations at frequencies higher than the rotation frequency of the blades. This behavior is analogous to the effect observed for wet systems in the experiments of Lekhal et al.[15] where higher velocity fluctuations were observed with increased moisture levels. These higher frequency fluctuations are associated with surface avalanching. The Fourier transform peak height for these fluctuations is significantly smaller than the main peak height

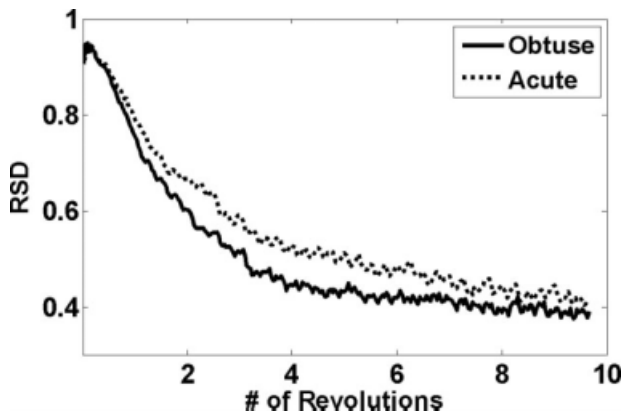

Figure 8. Effect of blade orientation on degree of mixing at 20 RPM.

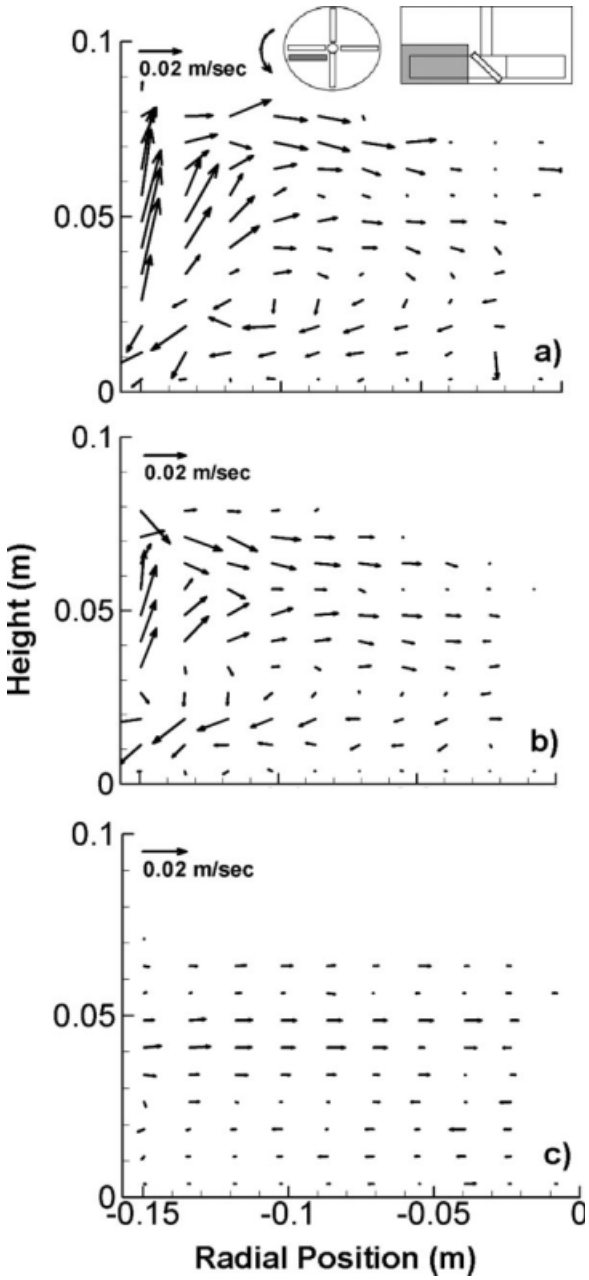

Figure 9. Time-averaged velocity fields in-front of blade.

Obtuse blade pitch: (a) $\mu_s = 0.5$, (b) $\mu_s = 0.3$, and (c) $\mu_s = 0.1$.

indicating that, while present, avalanching is not a dominant effect in this system.

The effect of sliding friction on the mixing kinetics can be seen in Figure 11. Relative standard deviation trends as a function of revolution number are shown in Figure 11a. Figure 11b shows some top view snapshots for each μ_s value. As expected, increasing the friction coefficient leads to enhanced mixing. Almost no mixing occurs at $\mu_s = 0.1$. After 5 revolutions the RSD values are 0.45 for $\mu_s = 0.5$ and 0.6 for $\mu_s = 0.3$ whereas the value for $\mu_s = 0.1$ remains at 0.9. This poor mixing performance is explained by the absence of the three-dimensional recirculation zone at $\mu_s = 0.1$. The presence of this vortex promotes convective mixing. However, in addition to convective mixing, diffusive mixing appears to play an important role in this system. Although little difference is observed between the recirculation patterns for $\mu_s = 0.5$ (Figure 9a) and $\mu_s = 0.3$ (Figure 9b), the RSD trends show a difference in mixing kinetics. The enhanced mixing performance observed at the higher μ_s value is explained by the higher granular temperature. These higher fluctuation velocities are associated with an increase in particle diffusivity. Thus, higher friction coefficients promote diffusive mixing. Although convective mixing is the dominant mechanism in this system, diffusive mixing becomes important when the homogenization process is down to the particle–particle level. However, the relative contribution of the diffusive and convective mixing components may change with particle/system size. Further work is needed to explore the effect of system size on the observed mixing kinetics.

Shear and normal stress profiles

In this section, we discuss the normal and shear stress profiles that develop inside bladed mixers. Stresses were calculated following the procedure outlined by Campbell.[32] Collisional stresses are obtained from

$$\tau_{ij} = \frac{d}{V_c}\langle F_i k_j \rangle \tag{12}$$

where d is the diameter of the particle, V_c is the size of the control volume, F_i is the total contact force, and k_j is the unit vector pointing along the line connecting the centers of the colliding particles. As before, $\langle\ \rangle$ represents the temporal averaging within the control volume. Stresses in granular systems are known to be scale-dependent.[33] As such, the calculated stress values are affected by the size of the control volume. The size of the control volume used here was determined by varying this parameter until the stress values obtained were independent of control volume size ($\sim$5 particle diameters). In this work, only the contribution of collisional stresses is considered as kinetic stresses were found to be 3 orders of magnitude smaller.

The collisional stress tensor was calculated in a three-dimensional cylindrical coordinate system. Our analysis showed that a symmetric stress tensor is obtained following this procedure (i.e., $\tau_{\theta r} = \tau_{r\theta}$). We focused our attention on the averaged normal stress and the shear stress component in the plane of the blade rotation, $\tau_{\theta r}$. From the normal stresses, the pressure inside the particle bed is given by

$$P = \frac{1}{3}\left(\tau_{\theta\theta} + \tau_{rr} + \tau_{yy}\right) \tag{13}$$

where $\tau_{\theta\theta}$, τ_{rr}, and τ_{yy} are the normal stresses in the tangential, radial, and vertical direction, respectively.

Figure 12 shows stress profiles at $r = 0.09$ m as a function of mixer height and number of revolutions for the obtuse blade pitch simulations at 20 RPM. The pressure profile is shown in Figure 12a and the $\tau_{\theta r}$ profile is shown in Figure 12c. These profiles document a periodic behavior similar to that of the velocity and density profiles. As demonstrated before, the main fluctuation frequency is equal to that of the blade rotation. The pressure profile implies that the material compresses when the blades are present and

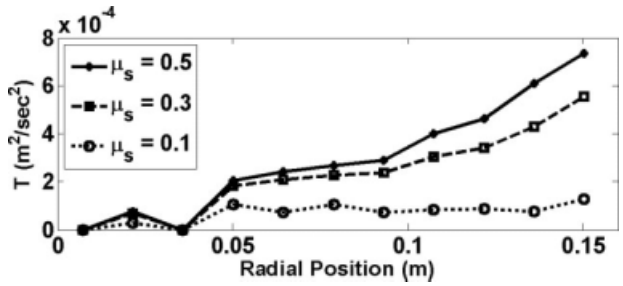

Figure 10. Time-averaged granular temperature profiles for different μ_s.

Solid line with solid dots shows the granular temperature for $\mu_s = 0.5$, dash line with squares $\mu_s = 0.3$, and dotted line with circles $\mu_s = 0.1$.

dilates in between blade passes. The mean and amplitude of the pressure fluctuations are a strong function of mixer height, as shown by the power spectrum (Figure 12b). Higher pressures are observed near the bottom plate and the pressure decreases monotonically with increased height, as the particles at the bottom sustain the weight of the particles at the top. This is similar to the behavior observed in

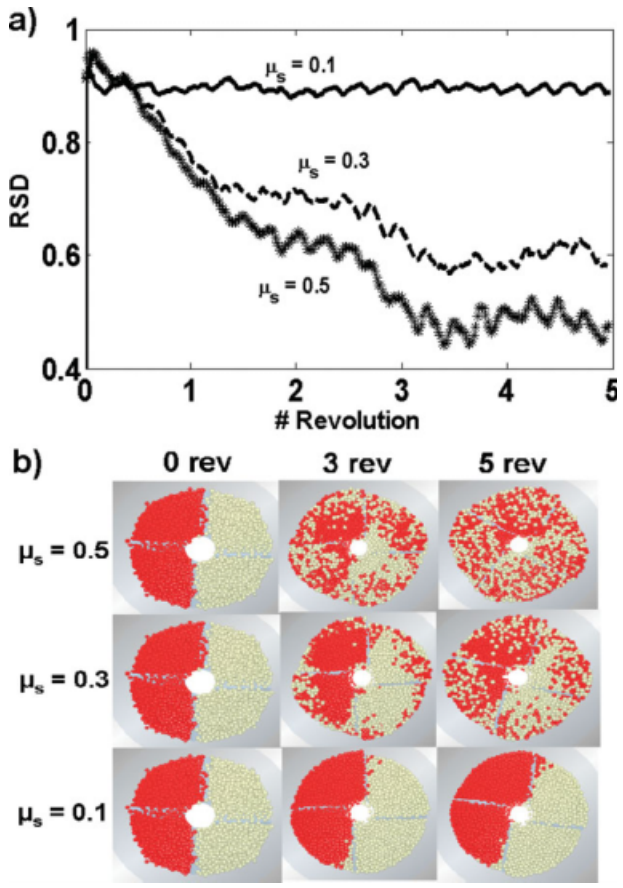

Figure 11. Effect of particle friction on mixing kinetics.

(a) Relative standard deviation for red particle concentration and (b) top view snapshot of mixing patterns for different friction coefficients. [Color figure can be viewed in the online issue, which is available at www.interscience.wiley.com.]

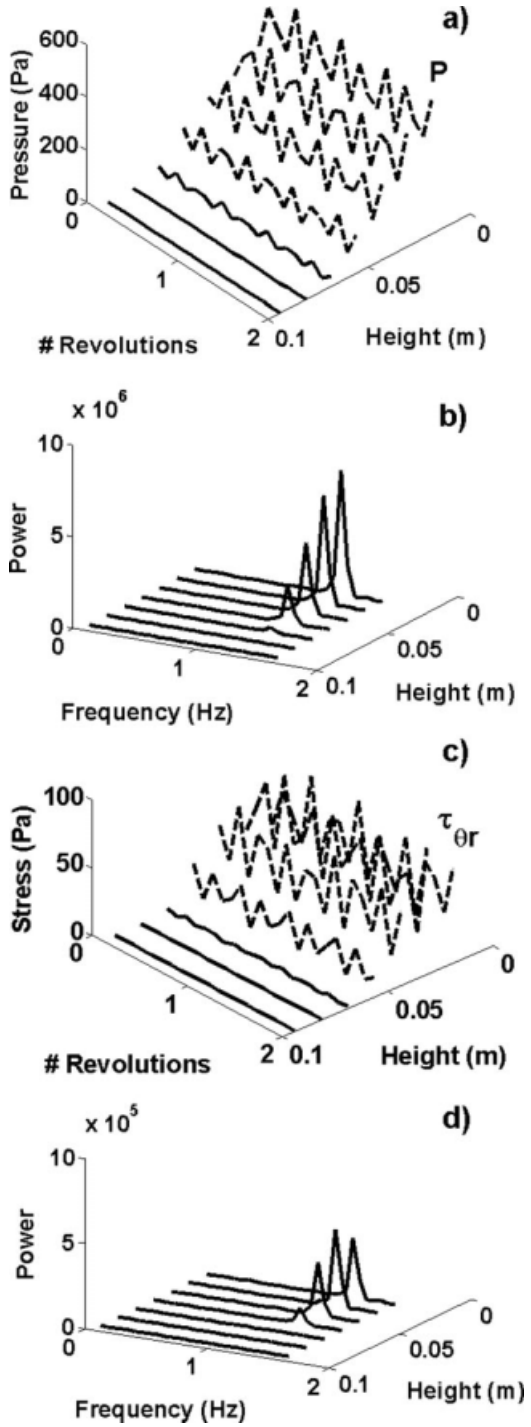

Figure 12. Pressure and shear stress fluctuations at r = 0.09 m for obtuse blade pitch flow at 20 RPM.

(a) Pressure profiles, (b) pressure power spectrum, (c) shear stress $\tau_{\theta r}$ profile, and (d) $\tau_{\theta r}$ power spectrum. Particle diameter = 5 mm.

silos[34,35] for static systems. Higher fluctuation amplitudes are also observed near the bottom plate. In contrast to the density profiles, the pressure fluctuation amplitude reaches a minimum above the blade height, as these particles sustain lower weights than the bottom particles. The $\tau_{\theta r}$ fluctuations

(Figure 12c) result from the formation of internal force chains when the material compresses near the blades and the subsequent breakage of these force chains as the material dilates in between blade passes. The value of the shear stress component $\tau_{\theta r}$ is roughly one order of magnitude lower than that of the normal stress or pressure. The mean and amplitude of the $\tau_{\theta r}$ fluctuations change little within the span of the blades, whereas these values decrease above the blade (Figure 12d). This indicates that most of the material shearing occurs within the span of the blade. Similar periodic behavior was observed for the remaining stress tensor components (not shown). However, the values for $\tau_{\theta y}$ and τ_{ry} fluctuate around zero, whereas the values for $\tau_{\theta r}$ do not.

The blade orientation affects the magnitude of the shear stress and pressure inside the mixer (Figure 13). Time-averaged pressure profiles are shown in Figure 13a as a function of radial position for both the obtuse and acute blade pitch orientations. Higher pressures are observed for the acute blade pitch. Pressure values vary little in the radial direction. The increase in pressure is explained by the increased bulk density observed for acute blade pitch (see the Density and granular temperature profiles section). The acute blade pitch orientation compresses the granular bed by pushing it down as the blades rotate leading to higher pressures. On the other hand, dilation occurs for the obtuse blade orientation which reduces the pressure inside the particle bed. The effect of blade orientation is less pronounced for the shear stress $\tau_{\theta r}$ (Figure 13b). The values of $\tau_{\theta r}$ are highest near the cylinder wall and close to zero near the impeller shaft. This is due to the increased tangential movement observed near the wall and the increased strength of the force chains due to wall friction. The ratio of the shear stress to the normal stress is known as the bulk friction coefficient and is used to describe stresses at yield conditions in soil mechanics. This ratio is related to the internal angle of friction and is commonly

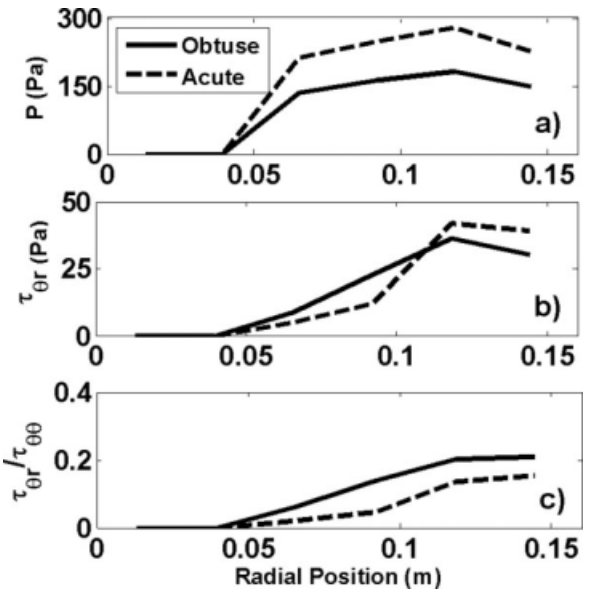

Figure 13. Comparison of time-averaged stresses for obtuse vs. acute blade pitch.

(a) Pressure, (b) shear stress$\tau_{\theta r}$ and (c) bulk friction coefficient $\tau_{\theta r}/\tau_{\theta\theta}$. Particle diameter = 5 mm.

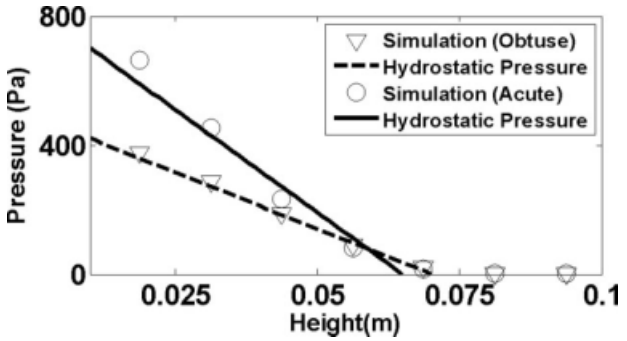

Figure 14. Time-averaged pressure as a function of height vs. hydrostatic pressure curves.

Particle diameter = 5 mm.

assumed to be a constant material property when the material is at the critical state.[36] The critical state of a granular material is characterized by a constant bulk density. Figure 13c shows the time averaged value of the $\tau_{\theta r}/\tau_{\theta\theta}$ ratio. This ratio is far from constant with maximum values near the cylinder wall. Nonconstant bulk friction coefficient values were also observed in computer simulations of two-dimensional hopper discharge.[37] The nonconstant bulk friction coefficient is most likely due to the changes in bulk density that occur within the particle bed as the blades rotate. These results suggest that the continuum models based on plasticity theory and soil mechanics may not provide an adequate description of granular flows in bladed mixers. The increase in bulk friction coefficient is a result of increased shear stresses near the cylinder wall. It should be noted that the highest value of the bulk friction coefficient is less than the particle–particle friction coefficient (0.3 for these simulations). This indicates that the particle bed yields at lower stresses than what is predicted by Coulomb's law. Identical friction coefficients are obtained from the $\tau_{\theta r}/\tau_{rr}$ ratio. The magnitude of τ_{yr}/τ_{rr} and $\tau_{\theta y}/\tau_{yy}$ is about 25% of the $\tau_{\theta r}/\tau_{\theta\theta}$ magnitude.

Despite the complex dynamics observed in the bladed mixer, we find that we can approximate the temporal averaged pressure as a function of mixer height with the simple hydrostatic pressure relationship

$$P = \rho_{\text{bulk}} g(h - H_{\text{bed}}) \tag{14}$$

where ρ_{bulk} is the total average bulk density of the granular bed, g is the acceleration due to gravity, h is the vertical position, and H_{bed} is the total height of the particle bed. The term in parenthesis in Eq. 12 is needed to account for the bottom plate being located at $h = 0.0$ m. Figure 14 shows the fit between the pressure values obtained from the DEM simulations and the hydrostatic pressure curves for the obtuse and acute blade pitch cases. The bulk density values obtained from linear fitting of the hydrostatic pressure equation were 780 kg/m^3 for the obtuse blade pitch case and 1300 kg/m^3 for the acute blade pitch case. These values are close to the averaged densities calculated from the DEM simulations ($\sim$900 kg/m^3 for the obtuse case and $\sim$1100 kg/m^3 for the acute case). This demonstrates that if the average bulk density during flow is known, the averaged normal stress in this dynamic system can be approximated by hydrostatics. This linear dependence of normal stresses with height has also been

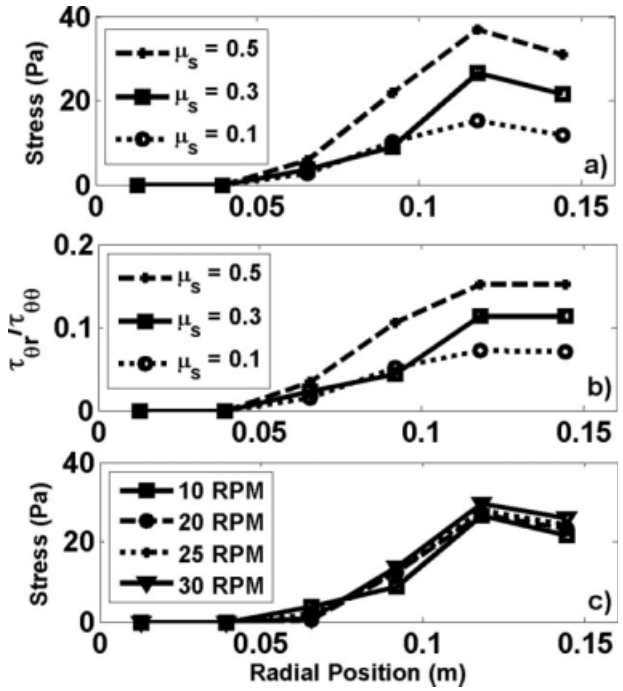

Figure 15. Effect of μ_s and shear rate on $\tau_{\theta r}$.

Particle diameter = 10 mm.

observed in fluidized systems.[38,39] However, further work is needed to explore the effect of particle/system size on the observed pressure profiles.

Many of the stress trends observed in the bladed mixer are consistent with the behavior of slowly deforming, quasi-static systems. In quasi-static systems, momentum transfer is governed by the frictional contacts between particles. As such, the particle–particle friction coefficient has a significantly effect on the developed shear stresses. Figure 15a shows the effect of interparticle friction on averaged values of $\tau_{\theta r}$ in the bladed mixer. Increasing the friction coefficient leads to an increase in shear stress. The $\tau_{\theta r}/\tau_{\theta\theta}$ ratio also increases with increased particle–particle friction (Figure 15b). The pressure profiles were found to be less sensitive to the particle's frictional characteristics. The strength and stability of the force chains that develop inside the mixer increase at higher friction coefficient. This result implies that the main source of stress in the bladed mixer is the formation of these force chains. On the other hand, shear stress profiles were found to be independent of shear rate (Figure 15c). From this we can conclude that increasing the shear rate in the bladed mixer leads to an increase in the shear stress fluctuation frequencies but has little effect on the mean and amplitude of these fluctuations. Momentum transfer is therefore governed by interparticle contacts and for our simulations the bladed mixer operates in the quasi-static regime. Knowledge of the flow regime in which a process takes places could assist during process design and scale-up as it provides a fundamental basis for granular flow behavior and could assist in identification of critical process parameters.

Conclusions

The discrete element method was used to characterize the flow of cohensionless, monodisperse spheres in a bladed mixer. The simulation results presented here are consistent with published experimental data and comparable to results obtained from previous numerical studies in similar systems. Instantaneous, averaged and fluctuating velocity fields show that the particle movement is governed by the angular motion of the blades. The granular bed deforms by forming heaps where the blades are present and valleys between blades passes. The presence of these heaps leads to the formation of a three-dimensional recirculation zone in front of the blade, where particles flow upward by the wall and downward by the impeller shaft. This 3-D recirculation promotes radial and vertical mixing. When the blade orientation is changed from an obtuse blade pitch to an acute blade pitch, the recirculation zone is not present. As a result, the particles move mainly in the tangential direction with little radial and vertical mixing. Acute blade pitch flows were shown to lower the granular temperature within the particle bed. This decrease in granular temperature is associated with a decrease in particle diffusivity. Diffusive mixing is therefore hindered by acute blade flows.

Density fluctuations exits within the granular bed with a frequency equal to the rotation frequency of the blades. This behavior indicates that the granular material compresses as the blade passes and dilates in between the blades. The system's frictional characteristics were shown to strongly influence the flow structure and mixing kinetics observed within the mixer. At low friction coefficients the 3-D recirculation in front of the blade is not present, reducing the convective mixing. Higher friction coefficients lead to an increase in diffusive mixing. Collisional stresses showed a periodic behavior similar to the density trends. Normal stresses were found to be an order of magnitude larger than shear stresses. The average pressure was found to vary with mixer height with maximum values near the bottom plate and could be approximated by the simple hydrostatic pressure. A higher bulk density was observed for the acute blade pitch which led to an increase in pressure for this blade orientation.

A strong dependence between the magnitude of the shear stresses and the friction coefficient of the particles was found. Shear stress increases with higher particle–particle friction. Surprisingly shear stresses were found to be independent of shear rate. These stress tensor characteristics indicate that for our simulations the granular flow in this bladed mixer occurs in the quasi-static regime. Momentum transfer in this system is therefore governed by interparticle contacts. This observation implies that quasi-static theories could provide a first-principles approach to bladed mixer design, scale-up, and operation for cohensionless systems. Many questions remain unanswered regarding the behavior of more complex granular systems in bladed mixers such as polydisperse systems, nonspherical particle beds, and wet systems. Additionally, a more comprehensive study exploring the effect of system size on the trends reported here is needed. Our study describes the behavior of an idealized granular system (cohesionless, monodisperse glass spheres in the millimeter size range) in a bladed mixer. Although simple in nature, it complements our understanding of granular flows in an industrially relevant geometry and represents an initial step toward understanding the granular behavior of more complex systems.

Acknowledgments

B.R. wishes to thank Bristol-Myers Squibb, Co. for financial support during an educational leave of absence. The authors would like to thank DEM Solutions for their support of this work. This work was partially supported by the National Science Foundation.

Literature Cited

1. Geldart D. *Powder Processing - The Overall View. Principles of Particle Technology*, 1st ed. Wiley, 1990:1–7.
2. Lekhal A, Girard KP, Brown MA, Kiang S, Glasser BJ, Khinast JG. Impact of agitated drying on crystal morphology: KCl-water system. *Powder Technol*. 2003;132:119–130.
3. Lee T, Lee J. Particle attrition by particle-surface friction in dryers. *Pharm Technol*. 2003;27:64–72.
4. Lekhal A, Girard KP, Brown MA, Kiang S, Khinast JG, Glasser BJ. The effect of agitated drying on the morphology of L-threonine (needle-like) crystals. *Int J Pharm*. 2004;270:263–277.
5. Bagster DF, Bridgwater J. The measurement of the force needed to move blades through a bed of cohesionless granules. *Powder Technol*. 1967;1:189–198.
6. Bagster DF, Bridgwater J. The flow of granular material over a moving blade. *Powder Technol*. 1970;3:323–338.
7. Malhotra K, Mujumdar AS, Imakoma H, Okazaki M. Fundamental particle mixing studies in an agitated bed of granular materials in a cylindrical vessel. *Powder Technol*. 1988;55:107–114.
8. Malhotra K, Mujumdar AS. Particle mixing and solids flowability in granular beds stirred by paddle-type blades. *Powder Technol*. 1990; 61:155–164.
9. Malhotra K, Mujumdar AS, Okazaki M. Particle flow patterns in a mechanically stirred two-dimensional cylindrical vessel. *Powder Technol*. 1990;60:179–189.
10. Laurent BFC, Bridgwater J, Parker DJ. Motion in a particle bed agitated by a single blade. *AIChE J*. 2000;46:1723–1734.
11. Jones JR, Parker DJ, Bridgwater J. Axial mixing in a ploughshare mixer. *Powder Technol*. 2007;178:73–86.
12. Bridgwater J, Broadbent CJ, Parker DJ. Study of the influence of blade speed on the performance of a powder mixer using positron emission particle tracking. *Chem Eng Res Des Part A: Trans Inst Chem Eng*. 1993;71:675–681.
13. Stewart RL, Bridgwater J, Parker DJ. Granular flow over a flat-bladed stirrer. *Chem Eng Sci*. 2001;56:4257–4271.
14. Conway SL, Lekhal A, Khinast JG, Glasser BJ. Granular flow and segregation in a four-bladed mixer. *Chem Eng Sci*. 2005;1260:7091–7107.
15. Lekhal A, Conway SL, Glasser BJ, Khinast JG. Characterization of granular flow of wet solids in a bladed mixer. *AIChE J*. 2006;52: 2757–2766.
16. Stewart RL, Bridgwater J, Zhou YC, Yu AB. Simulated and measured flow of granules in a bladed mixer—a detailed comparison. *Chem Eng Sci*. 2001;56:5457–5471.
17. Zhou YC, Yu AB, Bridgwater J. Segregation of binary mixture of particles in a bladed mixer. *J Chem Technol Biotechnol*. 2003;78:187–193.
18. Zhou YC, Yu AB, Stewart RL, Bridgwater J. Microdynamic analysis of the particle flow in a cylindrical bladed mixer. *Chem Eng Sci*. 2004;59:1343–1364.
19. Sinnott M, Cleary P. *3D DEM Simulations of a High Shear Mixer*. Paper presented at: Third International Conference on CFFD in the Minerals and Processing Industries, Melbourne, Victoria, Australia, CSIRO Materials 2006.
20. Tsuji Y, Tanaka T, Ishida T. Lagrangian numerical simulation of plug flow of cohesionless particles in a horizontal pipe. *Powder Technol*. 1992;71:239–250.
21. Gyenis J, Ulbert Z, Szépvölgyi J, Tsuji Y. Discrete particle simulation of flow regimes in bulk solids mixing and conveying. *Powder Technol*. 1999;104:248–257.
22. Limtrakul S, Boonsrirat A, Vatanatham T. DEM modeling and simulation of a catalytic gas-solid fluidized bed reactor: a spouted bed as a case study. *Chem Eng Sci*. 2004;59:5225–5231.
23. Limtrakul S, Chalermwattanatai A, Unggurawirote K, Tsuji Y, Kawaguchi T, Tanthapanichakoon W. Discrete particle simulation of solids motion in a gas-solid fluidized bed. *Chem Eng Sci*. 2003; 58:915–921.
24. Kruggel-Emden H, Simsek E, Rickelt S, Wirtz S, Scherer V. Review and extension of normal force models for the discrete element method. *Powder Technol*. 2007;171:157–173.
25. Kruggel-Emden H, Wirtz S, Scherer V. A study on tangential force laws applicable to the discrete element method (DEM) for materials with viscoelastic or plastic behavior. *Chem Eng Sci*. 2008;63:1523–1541.
26. Mindlin RD. Compliance of elastic bodies in contact. *J Appl Mech*. 1949;16:259–268.
27. Chung YC, Ooi JY. Influence of discrete element model parameters on bulk behavior of a granular solid under confined compression. *Particulate Sci Technol*. 2008;26:83–96.
28. Jaworski Z, Dyster KN, Nienow AW. The effect of size, location and pumping direction of pitched blade turbine impellers on flow patterns: LDA measurements and CFD predictions. *Chem Eng Res Des*. 2001;79:887–894.
29. Campbell CS. Self-diffusion in granular shear flows. *J Fluid Mech*. 1997;348:85–101.
30. Liu X, Metzger M, Glasser BJ. Couette flow with a bidisperse particle mixture. *Phys Fluids*. 2007;19:073301.
31. Forterre Y, Pouliquen O. Longitudinal vortices in granular flows. *Phys Rev Lett*. 2001;86:5886–5889.
32. Campbell CS. Granular shear flows at the elastic limit. *J Fluid Mech*. 2002;465:261–291.
33. Glasser BJ, Goldhirsch I. Scale dependence, correlations, and fluctuations of stresses in rapid granular flows. *Phys Fluids*. 2001;13: 407–420.
34. Sperl M. Experiments on corn pressure in silo cells—translation and comment of Janssen's paper from 1895. *Granular Matter*. 2006;8: 59–65.
35. Masson S, Martinez J. Effect of particle mechanical properties on silo flow and stresses from distinct element simulations. *Powder Technol*. 2000;109:164–178.
36. Jackson R. Some features of the flow of granular materials and aerated granular materials. *J Rheol*. 1985;30:907–930.
37. Potapov AV, Campbell CS. Computer simulation of hopper flow. *Phys Fluids*. 1996;8:2884–2894.
38. Tardos GI, McNamara S, Talu I. Slow and intermediate flow of a frictional bulk powder in the Couette geometry. *Powder Technol*. 2003;131:23–39.
39. Tardos GI, Khan MI, Schaeffer DG. Forces on a slowly rotating, rough cylinder in a Couette device containing a dry, frictional powder. *Phys Fluids*. 1998;10:335–341.

Manuscript received Jul. 8, 2008, revision received Oct. 17, 2008, and final revision received Feb. 12, 2009.